Universal hyperparallel hybrid photonic quantum gates with dipole-induced transparency in the weak-coupling regime*

Bao-Cang Ren, Guan-Yu Wang, and Fu-Guo Deng†
Department of Physics, Applied Optics Beijing Area Major Laboratory, Beijing Normal University, Beijing 100875, China
(Dated: April 2, 2015)

We present the dipole induced transparency (DIT) of a diamond nitrogen-vacancy center embedded in a photonic crystal cavity coupled to two waveguides, and it is obvious with the robust and flexible reflectance and transmittance difference of circularly polarized lights between the uncoupled and the coupled cavities even in the bad cavity regime (the Purcell regime). With this DIT, we propose two universal hyperparallel hybrid photonic quantum logic gates, including a hybrid hyper-controlled-not gate and a hybrid hyper-Toffoli gate, on photon systems in both the polarization and the spatial-mode degrees of freedom (DOFs), which are equal to two identical quantum logic gates operating simultaneously on the systems in one DOF. They can be used to perform more quantum operations with less resources in the quantum information protocols with multi-qubit systems in several DOFs, which may depress the resources consumed and the photonic dissipation. Moreover, they are more robust against asymmetric environment noise in the weak-coupling regime, compared with the integration of two cascaded quantum logic gates in one DOF.

PACS numbers: 03.67.Lx, 42.50.Ex, 42.50.Pq, 78.67.Hc

arXiv:1411.0274v3 [quant-ph] 1 Apr 2015

I. INTRODUCTION

The quantum computer is powerful in quantum information processing because of its fascinating capability of parallel computing, according to quantum mechanics theory [1]. Quantum logic gates are the key elements to precisely control and manipulate quantum states in quantum computation. Many proposals have been proposed to implement quantum logic gates with several physical systems both in theory and in experiment [2], such as the ion trap [3], nuclear magnetic resonance [4], quantum dot [5], superconducting qubits [6], and photon systems [7–9]. In practice, there are still several obstacles required to be overcome in the implementation of universal quantum logic gates, especially for the interaction between qubits. The optical nonlinearity of cavity quantum electrodynamics (QED) holds great promise for photon-photon, photon-dipole, and dipole-dipole interactions, and it has been used to complete some important tasks in quantum information processing, such as entanglement generation [10–12] and quantum logic gates [9, 13, 14].

Usually, the approaches for light-dipole interaction in cavity QED are focused on the strong-coupling regime [9, 11, 15], which is always referred to the high-Q regime with the vacuum Rabi frequency of a dipole (g) beyond both the cavity and the dipole decay rates. The strong coupling between a single atom and a photon has been demonstrated experimentally with cavity QED in the past few years [16, 17], and it has been used to implement the quantum logic gate between a single photon and a single trapped atom in experiment recently [17]. In a bad cavity regime, called the Purcell regime [18] with the cavity decay rate much bigger than the dipole decay rate, the interesting nonlinear optical property can also be observed with a much smaller coupling strength g. With the Purcell effect, the dipole-induced transparency (DIT) can be used for quantum information processing in the weak-coupling regime (low-Q regime) [12, 13, 19]. The fiber-optical switch [20] and the quantum phase switch [21] for photons have been demonstrated experimentally in the Purcell regime.

A nitrogen vacancy (NV) center in diamond is a promising candidate for a solid-state matter qubit (a dipole emitter) in cavity QED due to its long electron-spin decoherence time even at room temperature [22]. The approaches about an NV center in diamond coupled to an optical cavity (or a nanomechanical resonator) have been investigated both in theory [23] and in experiment [24–28]. The NV-center spins in diamonds are very useful in quantum networks for algorithms and quantum memories [29, 30]. The quantum entanglement between the polarization of a single photon and the electron spin of an NV center in diamond has been produced in experiment [31], and the Faraday effect induced by the single spin of an NV center in diamond coupling to light has been observed in experiment as well [32], which have facilitating applications in quantum information processing.

In this paper, we show that the DIT of a double-sided cavity-NV-center system (an NV center in diamond embedded in a photonic crystal cavity coupled to two waveguides) can be used for the photon-photon interaction in both the polarization and spatial-mode degrees of freedom (DOFs). In the Purcell regime, the DIT is still obvious with the robust and flexible reflectance and transmittance difference of circularly polarized lights between the uncoupled and the coupled cavities. With this DIT, we construct a hybrid polarization-spatial hyper-controlled-

*Published in Phys. Rev. A **91**, 032328 (2015)
†Corresponding author: fgdeng@bnu.edu.cn

not (CNOT) gate on a two-photon system, which is equal to two CNOT gates operating simultaneously on a four-photon system in one DOF. Also, we present a hybrid polarization-spatial hyper-Toffoli gate on a three-photon system and it is equal to two Toffoli gates on a six-photon system in one DOF. These universal hyperparallel hybrid photonic quantum gates can reduce the resources consumed in quantum information processing, and they are more robust against the photonic dissipation noise, compared with the integration of two cascaded quantum logic gates in one DOF. They have high fidelities in the symmetrical regime of double-sided cavity-NV-center systems and they can depress the asymmetric environment noise in the weak-coupling regime with a small Purcell factor. They can form universal hyperparallel photonic quantum computing assisted by single-photon rotations. Besides, they are useful for the quantum information protocols with multi-qubit systems in several DOFs, for example, the preparation of two-photon hyperentangled states and the complete analysis for them.

II. DIT FOR DOUBLE-SIDED CAVITY-NV-CENTER SYSTEM

A negatively charged NV center in diamond consists of a substitutional nitrogen atom, an adjacent vacancy, and six electrons coming from the nitrogen atom and three carbon atoms surrounding the vacancy. Its ground state is an electron-spin triplet with the splitting at 2.88 GHz between the magnetic sublevels $|0\rangle$ ($|m_s=0\rangle$) and $|\pm1\rangle$ ($|m_s=\pm1\rangle$). There are six electronic excited states according to the Hamiltonian with the spin-orbit and spin-spin interactions and C_{3v} symmetry [33]. Optical transitions between the ground states and the excited states are spin preserving, while the electronic orbital angular momentum is changed by the photon polarization. The excited state $|A_2\rangle$, which is robust with the stable symmetric properties, decays with an equal probability to the ground states $|-1\rangle$ and $|+1\rangle$ through the σ^+ and σ^- polarization radiations, respectively [31] (see Fig.1(b)). The excited state $|A_2\rangle$ has the form $|A_2\rangle=(|E_-\rangle|+1\rangle+|E_+\rangle|-1\rangle)/\sqrt{2}$ [31], where $|E_\pm\rangle$ are the orbit states with the angular momentum projections ±1 along the NV axis (the z axis in Fig.1). The ground states are associated with the orbit state $|E_0\rangle$ with the angular momentum projection zero along the NV axis.

The DIT of the cavity-NV-center system (shown in Fig.1(a)) can be calculated by the Heisenberg equations of motion for the cavity field operator $\hat{a}$ and the dipole operator $\hat{\sigma}_-$ [12, 34], that is,

$$\begin{aligned}\frac{d\hat{a}}{dt}=&-\left[i(\omega_c-\omega)+\eta+\frac{\kappa}{2}\right]\hat{a}-\sqrt{\eta}(\hat{a}_{in}+\hat{a}'_{in})\\&-g\hat{\sigma}_--\hat{h},\\\frac{d\hat{\sigma}_-}{dt}=&-\left[i(\omega_k-\omega)+\frac{\gamma}{2}\right]\hat{\sigma}_--g\hat{\sigma}_z\hat{a}-\hat{f}.\end{aligned}\tag{1}$$

Here, ω_k ($k=-1,+1$), ω, and ω_c are the frequencies of the transition between $|-1\rangle$ ($|+1\rangle$) and $|A_2\rangle$, the waveguide channel mode, and the cavity mode, respectively. g is the coupling strength of the cavity to the NV center. $\gamma/2$ is the decay rate of the emitter. η and $\kappa/2$ are the decay rates of the cavity field into waveguide channel modes and cavity intrinsic loss modes, respectively. $\hat{g}$ and $\hat{f}$ are noise operators, which can preserve the commutation relation. The operators $\hat{a}_{in}$ ($\hat{a}'_{in}$) and $\hat{a}_{out}$ ($\hat{a}'_{out}$) are the input and output field operators, respectively. They satisfy the boundary relations $\hat{a}_{out}=\hat{a}_{in}+\sqrt{\eta}\,\hat{a}$ and $\hat{a}'_{out}=\hat{a}'_{in}+\sqrt{\eta}\,\hat{a}$. The decay rates of the cavity field into two waveguides can be set very close to get approximately the same fidelity for both directions ($\eta_1\cong\eta_2=\eta$) [16]. In the weak excitation limit with the emitter predominantly in the ground state ($\langle\sigma_z\rangle=-1$), the transmission and reflection coefficients of the cavity-NV-center system are given by

$$\begin{aligned}t(\omega)&=\frac{-\eta[i(\omega_k-\omega)+\frac{\gamma}{2}]}{[i(\omega_k-\omega)+\frac{\gamma}{2}][i(\omega_c-\omega)+\eta+\frac{\kappa}{2}]+g^2},\\r(\omega)&=1+t(\omega).\end{aligned}\tag{2}$$

Considering the emitter is resonant with the cavity mode ($\omega_c=\omega_k=\omega$), the reflection and transmission coefficients are $t=-(2F_p+1+\frac{\lambda}{2})^{-1}$ and $r=(2F_p+\frac{\lambda}{2})/(2F_p+1+\frac{\lambda}{2})$ for $g>0$, and they are $t_0=-(1+\frac{\lambda}{2})^{-1}$ and $r_0=\frac{\lambda}{2}/(1+\frac{\lambda}{2})$ for $g=0$. Here $F_p=g^2/(\eta\gamma)$ is the Purcell factor ($\kappa\approx0$), and $\lambda=\kappa/\eta$. If the Purcell factor is $F_p\gg1$, the reflection and transmission coefficients are $r(\omega)\to1$ and $t(\omega)\to0$. If the cavity decay rate is $\lambda\ll1$, the reflection and transmission coefficients of the bare cavity are $r_0(\omega)\to0$ and $t_0(\omega)\to-1$ (Fig.2 (a)). The interaction between a single photon and the emitter in an NV center is obtained as

$$\begin{aligned}|\sigma^+\rangle(|-1\rangle+|+1\rangle)&\to|\sigma_r^+\rangle|-1\rangle-|\sigma_{t_0}^+\rangle|+1\rangle,\\|\sigma^-\rangle(|-1\rangle+|+1\rangle)&\to-|\sigma_{t_0}^-\rangle|-1\rangle+|\sigma_r^-\rangle|+1\rangle.\end{aligned}\tag{3}$$

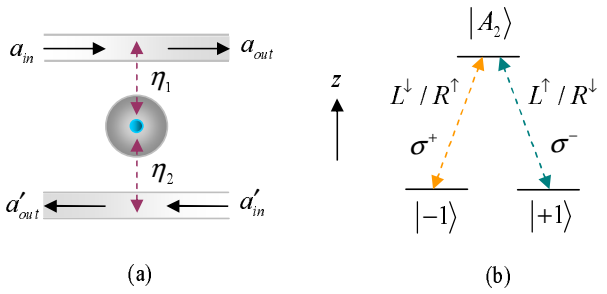

FIG. 1: (Color online) The optical transitions of an NV center with circularly polarized lights. (a) A double-sided cavity-waveguide-NV-center system. (b) The optical transitions of an NV center. The photon in the state $|R^\uparrow\rangle$ or $|L^\downarrow\rangle$ corresponds to σ^+, and the photon in the state $|R^\downarrow\rangle$ or $|L^\uparrow\rangle$ corresponds to σ^-. $R^\uparrow$ ($R^\downarrow$) and $L^\uparrow$ ($L^\downarrow$) represent the right- and left- circularly polarized lights with their input (output) directions parallel (antiparallel) to the z direction.

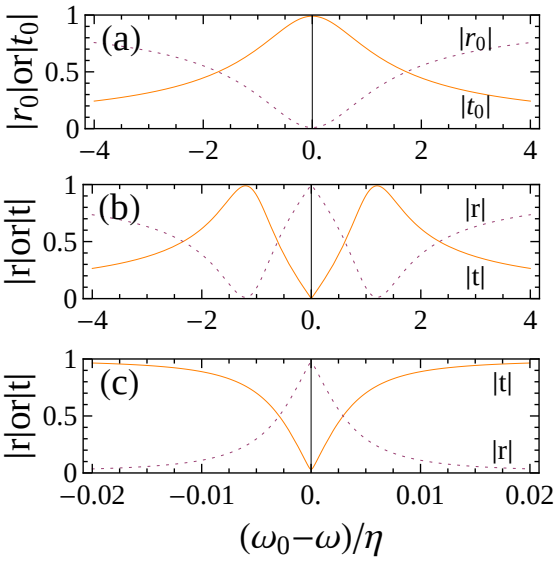

FIG. 2: (Color online) The reflection and transition coefficients of the double-sided cavity-NV-center system vs the normalized frequency detuning $(\omega-\omega_0)/\eta$ ($\omega_c=\omega_k=\omega_0$). (a) $g=0$, $\gamma\sim 2\pi\times 80$ MHz [27] and $\eta=50\kappa\sim 2\pi\times 0.05$ THz ($Q\sim 10^4$). (b) $g\sim 2\pi\times 0.06$ THz, $\gamma\sim 2\pi\times 80$ MHz, and $\eta=50\kappa\sim 2\pi\times 0.05$ THz. (c) $g\sim 2\pi\times 0.035$ THz, $\gamma\sim 2\pi\times 80$ MHz, and $\eta=50\kappa\sim 2\pi\times 0.5$ THz ($Q\sim 10^3$).

Here the subscript r (t_0) represents the photon reflected (transmitted).

In the strong-coupling (high-Q) regime, the dipole-induced reflection is the result of vacuum Rabi splitting with the Rabi frequency $\Omega=2g$, and the transmission (reflection) dip is equal to $2g$ (Fig.2(b)). The incoming pulse must be longer than the Rabi oscillation period $1/g$ in this high-Q regime [12]. In the weak-coupling (low-Q) regime, the dipole-induced reflection is caused by the destructive interference of the cavity field and the dipole emission field, and the transmission (reflection) dip is equal to $2\Gamma=2F_p\gamma/(1+\frac{\lambda}{2})$ (Fig.2(c)). The incoming pulse must be longer than the Rabi oscillation period $1/\Gamma$ in this bad cavity regime [12]. In the weak excitation approximation, the time interval between two photons should be longer than $\Delta\tau=2F_p/[\gamma(1+\frac{\lambda}{2})]$.

The transmission and reflection rule in Eq.(3) can be described in the circular basis $\{|R\rangle,|L\rangle\}$ shown in Fig.1(b). The photon circular polarization is usually related to the direction propagation, and the handedness circular polarized light is changed after reflection. That is,

$$\begin{aligned}
&|R^{\uparrow},-1\rangle \rightarrow |L^{\downarrow},-1\rangle, \quad |R^{\uparrow},+1\rangle \rightarrow -|R^{\uparrow},+1\rangle,\\
&|L^{\downarrow},-1\rangle \rightarrow |R^{\uparrow},-1\rangle, \quad |L^{\downarrow},+1\rangle \rightarrow -|L^{\downarrow},+1\rangle,\\
&|R^{\downarrow},-1\rangle \rightarrow -|R^{\downarrow},-1\rangle, \quad |R^{\downarrow},+1\rangle \rightarrow |L^{\uparrow},+1\rangle,\\
&|L^{\uparrow},-1\rangle \rightarrow -|L^{\uparrow},-1\rangle, \quad |L^{\uparrow},+1\rangle \rightarrow |R^{\downarrow},+1\rangle.
\end{aligned} \tag{4}$$

Here, in the left-hand side of "$\rightarrow$" in Eq.(4), $|R^{\uparrow}\rangle$ ($|L^{\uparrow}\rangle$) represents that the photon R (L) is put into the cavity-NV-center system through the down spatial mode of the cavity-NV-center system, and $|R^{\downarrow}\rangle$ ($|L^{\downarrow}\rangle$) represents that the photon R (L) is put into the cavity-NV-center system through the upper spatial mode of the cavity-NV-center system. In the right-hand side of "$\rightarrow$" in Eq.(4), $|R^{\uparrow}\rangle$ ($|L^{\uparrow}\rangle$) represents that the photon R (L) exits from the cavity-NV-center system through the upper spatial mode of the cavity-NV-center system, and $|R^{\downarrow}\rangle$ ($|L^{\downarrow}\rangle$) represents that the photon R (L) exits from the cavity-NV-center system through the down spatial mode of the cavity-NV-center system. i_1 and i_2 represent the two spatial modes of photon i ($i=a,b$) as shown in Fig.3.

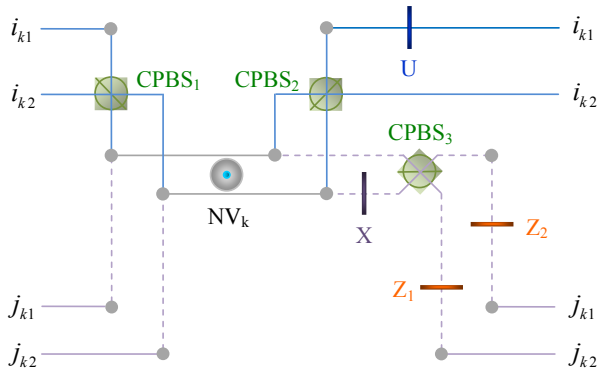

FIG. 3: (Color online) Schematic diagram for a hybrid photonic hyper-CNOT gate operating on a two-photon system in both the spatial-mode and polarization DOFs. X represents a half-wave plate which is used to perform a polarization bit-flip operation $X=|R\rangle\langle L|+|L\rangle\langle R|$. Z_n ($n=1,2$) represents a half-wave plate which is used to perform a polarization phase-flip operation $Z=|R\rangle\langle R|-|L\rangle\langle L|$. U represents a wave plate which is used to perform a polarization phase-flip operation $U=-|R\rangle\langle R|-|L\rangle\langle L|$. CPBS$_m$ ($m=1,2,3$) represents a polarizing beam splitter in the circular basis, which transmits the photon in right-circular polarization $|R\rangle$ and reflects the photon in left-circular polarization $|L\rangle$, respectively. i_{k1} and i_{k2} represent the two spatial modes of photon i ($i=a,b$), respectively. NV$_k$ ($k=1,2$) represents a double-sided cavity-NV-center system. An optical switch is used in the merging point of i_{kl} and j_{kl}.

III. HYBRID PHOTONIC HYPER-CNOT GATE ON A TWO-PHOTON SYSTEM

Here, a hybrid photonic hyper-CNOT gate on a two-photon system in both the polarization and spatial-mode DOFs is used to complete the task that a bit-flip operation is performed on the spatial mode of photon b (the target qubit) when the polarization of photon a (the control qubit) is in the state $|L\rangle$, and simultaneously a bit-flip operation takes place on the spatial mode of photon a when the polarization of photon b is in the state $|L\rangle$. It can act as two cascaded hybrid CNOT gates on a four-photon system in one DOF with less operation time and less resources, which is far different from the hybrid

CNOT gate based on one DOF of photon systems [35]. The principle of our hybrid photonic hyper-CNOT gate is shown in Fig.3, where two identical quantum circuits are required. We describe it in detail as follows.

Suppose that the initial states of the two NV centers are $|+\rangle_{e_1}$ and $|+\rangle_{e_2}$, respectively, and the initial states of the two photons a and b are

$$\begin{aligned} |\psi_a\rangle_0 &= (\alpha_1|R\rangle + \alpha_2|L\rangle)_a(\gamma_1|a_1\rangle + \gamma_2|a_2\rangle), \\ |\psi_b\rangle_0 &= (\beta_1|R\rangle + \beta_2|L\rangle)_b(\delta_1|b_1\rangle + \delta_2|b_2\rangle). \end{aligned} \tag{5}$$

Here $|\pm\rangle = \frac{1}{\sqrt{2}}(|-1\rangle \pm |+1\rangle)$.

First, we perform the Hadamard operations on the polarization DOF of both photons a and b, and the states of the two photons a and b become $|\psi'_a\rangle_0 = (\alpha'_1|R\rangle + \alpha'_2|L\rangle)_a(\gamma_1|a_1\rangle + \gamma_2|a_2\rangle)$ and $|\psi'_b\rangle_0 = (\beta'_1|R\rangle + \beta'_2|L\rangle)_b(\delta_1|b_1\rangle + \delta_2|b_2\rangle)$. Here, $\alpha'_1 = \frac{1}{\sqrt{2}}(\alpha_1 + \alpha_2)$, $\alpha'_2 = \frac{1}{\sqrt{2}}(\alpha_1 - \alpha_2)$, $\beta'_1 = \frac{1}{\sqrt{2}}(\beta_1 + \beta_2)$, and $\beta'_2 = \frac{1}{\sqrt{2}}(\beta_1 - \beta_2)$. The Hadamard operation on the polarization DOF of a photon is used to implement the unitary single-qubit operation $|R\rangle \to \frac{1}{\sqrt{2}}(|R\rangle + |L\rangle)$ and $|L\rangle \to \frac{1}{\sqrt{2}}(|R\rangle - |L\rangle)$. Subsequently, we lead the two wavepackets of photon a (b) from the two spatial modes $|a_1\rangle$ ($|b_1\rangle$) and $|a_2\rangle$ ($|b_2\rangle$) to spatial ports i_{11} (i_{21}) and i_{12} (i_{22}) of the cavity-NV-center system NV_1 (NV_2) as shown in Fig.3. After photon a (b) passes through CPBS_1, NV_1 (NV_2), CPBS_2, and U, the state of the quantum system composed of photon a (b) and NV_1 (NV_2) is transformed from $|\Psi'_{ae_1}\rangle_0 \equiv |\psi'_a\rangle_0 \otimes |+\rangle_{e_1}$ ($|\Psi'_{be_2}\rangle_0 \equiv |\psi'_b\rangle_0 \otimes |+\rangle_{e_2}$) to $|\Psi_{ae_1}\rangle_1$ ($|\Psi_{be_2}\rangle_1$). Here

$$\begin{aligned} |\Psi_{ae_1}\rangle_1 &= \frac{1}{\sqrt{2}}\{\gamma_1[|-1\rangle_{e_1}(\alpha'_1|R\rangle + \alpha'_2|L\rangle)_a \\ &\quad - |+1\rangle_{e_1}(\alpha'_2|R\rangle + \alpha'_1|L\rangle)_a]|a_1\rangle \\ &\quad + \gamma_2[|-1\rangle_{e_1}(\alpha'_2|R\rangle + \alpha'_1|L\rangle)_a \\ &\quad - |+1\rangle_{e_1}(\alpha'_1|R\rangle + \alpha'_2|L\rangle)_a]|a_2\rangle\}, \\ |\Psi_{be_2}\rangle_1 &= \frac{1}{\sqrt{2}}\{\delta_1[|-1\rangle_{e_2}(\beta'_1|R\rangle + \beta'_2|L\rangle)_b \\ &\quad - |+1\rangle_{e_2}(\beta'_2|R\rangle + \beta'_1|L\rangle)_b]|b_1\rangle \\ &\quad + \delta_2[|-1\rangle_{e_2}(\beta'_2|R\rangle + \beta'_1|L\rangle)_b \\ &\quad - |+1\rangle_{e_2}(\beta'_1|R\rangle + \beta'_2|L\rangle)_b]|b_2\rangle\}. \end{aligned} \tag{6}$$

Second, after a Hadamard operation is performed on NV_1 (NV_2), we let photon a (b) pass through two spatial paths j_{21} (j_{11}) and j_{22} (j_{12}) of the cavity-NV-center system NV_2 (NV_1) shown in Fig.3 (with optical switches). Here a Hadamard operation on an NV center is used to complete the transformations $|-1\rangle \to |+\rangle$ and $|+1\rangle \to |-\rangle$. After photon a (b) passes through NV_2 (NV_1), X, CPBS_3, Z_1, and Z_2, the state of the quantum system composed of photons a and b, NV_1, and NV_2 is changed from $|\Psi_{abe_1e_2}\rangle_1 \equiv |\Psi_{ae_1}\rangle_1 \otimes |\Psi_{be_2}\rangle_1$ to

$$\begin{aligned} |\Psi_{abe_1e_2}\rangle_2 = \frac{1}{2}&[|-1\rangle_{e_1}\alpha_2(|L\rangle - |R\rangle)_a(\delta_2|b_1\rangle + \delta_1|b_2\rangle) \\ &-|+1\rangle_{e_1}\alpha_1(|R\rangle + |L\rangle)_a(\delta_1|b_1\rangle + \delta_2|b_2\rangle)] \\ &\otimes[|-1\rangle_{e_2}\beta_2(|L\rangle - |R\rangle)_b(\gamma_2|a_1\rangle + \gamma_1|a_2\rangle) \\ &-|+1\rangle_{e_2}\beta_1(|R\rangle + |L\rangle)_b(\gamma_1|a_1\rangle + \gamma_2|a_2\rangle)]. \end{aligned} \tag{7}$$

At last, with the Hadamard operations performed on NV_1, NV_2, and the polarization DOF of photons a and b again, the outcome of a hybrid photonic hyper-CNOT gate can be obtained by measuring the two NV centers in the orthogonal basis $\{|-1\rangle, |+1\rangle\}$ and performing conditional phase shift operations on the polarization modes of photons a and b. After we perform an additional sign change $|L\rangle_a \to -|L\rangle_a$ on photon a when NV_1 is in the state $|+1\rangle_{e_1}$ and an addition sign change $|L\rangle_b \to -|L\rangle_b$ on photon b when NV_2 is in the state $|+1\rangle_{e_2}$, the state of the two-photon system ab becomes

$$\begin{aligned} |\psi_{ab}\rangle = &[\alpha_1|R\rangle_a(\delta_1|b_1\rangle + \delta_2|b_2\rangle) + \alpha_2|L\rangle_a(\delta_2|b_1\rangle + \delta_1|b_2\rangle)] \\ &\otimes[\beta_1|R\rangle_b(\gamma_1|a_1\rangle + \gamma_2|a_2\rangle) + \beta_2|L\rangle_b(\gamma_2|a_1\rangle + \gamma_1|a_2\rangle)]. \end{aligned} \tag{8}$$

It is the result of a hybrid photonic hyper-CNOT gate operating on a two-photon system, by using the polarization mode of one photon as the control qubit and the spatial mode of the other photon as the target qubit, respectively.

IV. HYBRID PHOTONIC HYPER-TOFFOLI GATE ON A THREE-PHOTON SYSTEM

A Toffoli gate is used to complete a bit-flip operation on the state of the target qubit when both two control qubits are in the state $|1\rangle$; otherwise, nothing is done on the target qubit [1]. It is a universal quantum gate for quantum computing. Here, the hybrid hyper-Toffoli gate, operating on a three-photon system abc in both the polarization and spatial-mode DOFs, is used to achieve the task that a bit-flip operation is performed on the spatial mode of photon c (the target qubit) when the polarizations of both photons a and b (the control qubits) are $|L\rangle$, and simultaneously a bit-flip operation takes place on the spatial mode of photon b (the target qubit) when the spatial mode of photon a is $|a_2\rangle$ and the polarization of photon c is $|L\rangle$ (the control qubits).

The two parts of the quantum circuit for our hybrid photonic hyper-Toffoli gate are shown in Fig.4 and Fig.5, respectively. Suppose that the initial states of the two NV centers are $|+\rangle_{e_1}$ and $|+\rangle_{e_2}$, respectively, and the initial states of three photons a, b, and c are $|\phi_a\rangle_0 = (\alpha_1|R\rangle + \beta_1|L\rangle)_a(\gamma_1|a_1\rangle + \delta_1|a_2\rangle)$, $|\phi_b\rangle_0 = (\alpha_2|R\rangle + \beta_2|L\rangle)_b(\gamma_2|b_1\rangle + \delta_2|b_2\rangle)$, and $|\phi_c\rangle_0 = (\alpha_3|R\rangle + \beta_3|L\rangle)_c(\gamma_3|c_1\rangle + \delta_3|c_2\rangle)$, respectively. This hyper-Toffoli

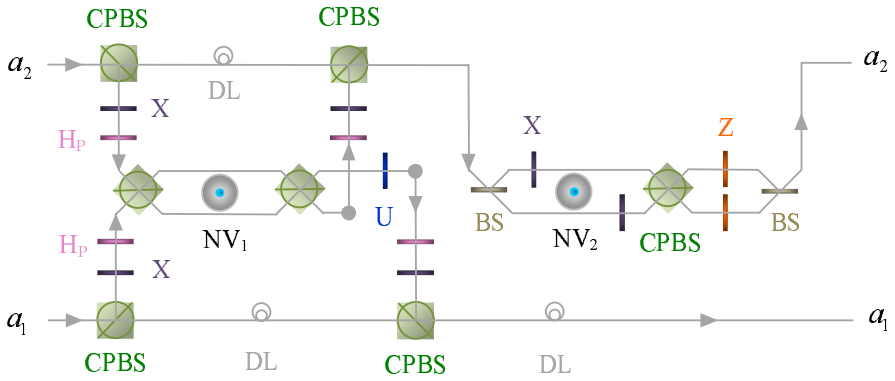

FIG. 4: (Color online) Schematic diagram for the first step of our hybrid photonic hyper-Toffoli gate operating on both the spatial-mode and polarization DOFs of a three-photon system. H_P represents a half-wave plate which is used to perform a polarization Hadamard operation on a photon. BS represents a 50:50 beam splitter which is used to perform a spatial-mode Hadamard operation on a photon $[|a_2\rangle \rightarrow \frac{1}{\sqrt{2}}(|a_1'\rangle + |a_2'\rangle)]$. DL represents a time-delay device.

gate can be constructed with two steps described in detail below.

The principle of the first step for our hybrid photonic hyper-Toffoli gate is shown in Fig.4. First, the wave packets of photon a from the two spatial modes $|a_1\rangle$ and $|a_2\rangle$ are led to CPBS, X, H_P, CPBS, NV_1, CPBS, U, H_P, X, and CPBS in sequence as shown in Fig.4, and the state of the quantum system composed of photon a and NV_1 is transformed from $|\Phi_{ae_1}\rangle_0 \equiv |\phi_a\rangle_0 \otimes |+\rangle_{e_1}$ to

$$|\Phi_{ae_1}\rangle_1 = (\alpha_1|R\rangle_a|+\rangle_{e_1} + \beta_1|L\rangle_a|-\rangle_{e_1})(\gamma_1|a_1\rangle + \delta_1|a_2\rangle). \tag{9}$$

Subsequently, we lead the wave packet of photon a from the spatial mode $|a_2\rangle$ to BS, X, NV_2, X, CPBS, Z, and BS in sequence as shown in Fig.4, and the state of the quantum system composed of photon a, NV_1, and NV_2 is transformed from $|\Phi_{ae_1e_2}\rangle_1 \equiv |\Phi_{ae_1}\rangle_1 \otimes |+\rangle_{e_2}$ to

$$\begin{aligned}|\Phi_{ae_1e_2}\rangle_2 &= (\alpha_1|R\rangle_a|+\rangle_{e_1} + \beta_1|L\rangle_a|-\rangle_{e_1}) \\ &\otimes (\gamma_1|a_1\rangle|+\rangle_{e_2} + \delta_1|a_2\rangle|-\rangle_{e_2}).\end{aligned} \tag{10}$$

In the second step, after a Hadamard operation is performed on each of NV_1 and NV_2, the two wave packets of photon b from the two spatial modes $|b_1\rangle$ and $|b_2\rangle$ are led to CPBSs, NV_1, CPBS, X, and U in sequence as shown in Fig.5, and the state of the quantum system composed of NV_1, NV_2, and photons a and b is transformed from $|\Phi_{abe_1e_2}\rangle_2 = |\Phi_{ae_1e_2}\rangle_2 \otimes |\phi_b\rangle_0$ to

$$\begin{aligned}|\Phi_{abe_1e_2}\rangle_3 = &(\alpha_1\beta_2|-1\rangle_{e_1}|RL\rangle_{ab} + \beta_1\beta_2|+1\rangle_{e_1}|LL\rangle_{ab} \\ &-\alpha_1\alpha_2|-1\rangle_{e_1}|RL\rangle_{ab} + \beta_1\alpha_2|+1\rangle_{e_1}|LR\rangle_{ab}) \\ &\otimes(\gamma_1|a_1\rangle|-1\rangle_{e_2} + \delta_1|a_2\rangle|+1\rangle_{e_2}) \\ &\otimes(\gamma_2|b_1\rangle + \delta_2|b_2\rangle).\end{aligned} \tag{11}$$

After a Hadamard operation is performed on NV_1, the two wave packets of photon b from the two spatial modes $|b_1\rangle$ and $|b_2\rangle$ are led to H_P, CPBS, NV_1, CPBS, X, and U in sequence with an optical switch S (through the dotted line in Fig.5), and then the state of the quantum system composed of NV_1, NV_2, and photons a and b becomes

$$\begin{aligned}|\Phi_{abe_1e_2}\rangle_4 = &[\alpha_1\beta_2|+\rangle_{e_1}|RL\rangle_{ab} + \beta_1\beta_2|-\rangle_{e_1}|LL\rangle_{ab} \\ &-\frac{\alpha_1\alpha_2}{\sqrt{2}}|+\rangle_{e_1}|R(R-L)\rangle_{ab} \\ &-\frac{\beta_1\alpha_2}{\sqrt{2}}|+\rangle_{e_1}|L(R+L)\rangle_{ab}] \\ &\otimes(\gamma_1|a_1\rangle|-1\rangle_{e_2} + \delta_1|a_2\rangle|+1\rangle_{e_2}) \\ &\otimes(\gamma_2|b_1\rangle + \delta_2|b_2\rangle).\end{aligned} \tag{12}$$

Next, after another Hadamard operation is performed on NV_1, we lead the wave packets of photon c from the two spatial modes $|c_1\rangle$ and $|c_2\rangle$ to X, U, NV_1, U, X, and CPBS in sequence as shown in Fig.5. The quantum system composed of NV_1, NV_2, and photons a, b, and c is evolved from $|\Phi_{abce_1e_2}\rangle_4 \equiv |\Phi_{abe_1e_2}\rangle_4 \otimes |\phi_c\rangle_0$ to

$$\begin{aligned}|\Phi_{abce_1e_2}\rangle_5 = &[\alpha_1\beta_2|-1\rangle_{e_1}|RL\rangle_{ab}(\gamma_3|c_2\rangle + \delta_3|c_1\rangle) \\ &+\beta_1\beta_2|+1\rangle_{e_1}|LL\rangle_{ab}(\gamma_3|c_1\rangle + \delta_3|c_2\rangle) \\ &-\frac{\alpha_1\alpha_2}{\sqrt{2}}|-1\rangle_{e_1}|R(R-L)\rangle_{ab}(\gamma_3|c_2\rangle + \delta_3|c_1\rangle) \\ &-\frac{\beta_1\alpha_2}{\sqrt{2}}|-1\rangle_{e_1}|L(R+L)\rangle_{ab}(\gamma_3|c_2\rangle + \delta_3|c_1\rangle)] \\ &\otimes(\gamma_2|b_1\rangle + \delta_2|b_2\rangle)(\gamma_1|a_1\rangle|-1\rangle_{e_2} \\ &+\delta_1|a_2\rangle|+1\rangle_{e_2})(\alpha_3|R\rangle + \beta_3|L\rangle)_c.\end{aligned} \tag{13}$$

Subsequently, the wave packets of photon b from the two spatial modes $|b_1\rangle$ and $|b_2\rangle$ are led to CPBS, NV_1, CPBS, X, and U (through the dash-dot-dotted line in Fig.5) after a Hadamard operation is performed on NV_1, and then the wavepackets of photon c from the two spatial modes $|c_1\rangle$ and $|c_2\rangle$ are led to CPBSs, NV_2, CPBS, X, and U in sequence as shown in Fig.5. The state of

the system $abce_1e_2$ is transformed from $|\Phi_{abce_1e_2}\rangle_5$ to

$$\begin{aligned}|\Phi_{abce_1e_2}\rangle_6 = &[\alpha_1\beta_2|+\rangle_{e_1}|RL\rangle_{ab}(\gamma_3|c_2\rangle+\delta_3|c_1\rangle)\\ &+\beta_1\beta_2|-\rangle_{e_1}|LL\rangle_{ab}(\gamma_3|c_1\rangle+\delta_3|c_2\rangle)\\ &-\frac{\alpha_1\alpha_2}{\sqrt{2}}|+\rangle_{e_1}|R(R-L)\rangle_{ab}(\gamma_3|c_2\rangle+\delta_3|c_1\rangle)\\ &+\frac{\beta_1\alpha_2}{\sqrt{2}}|-\rangle_{e_1}|L(R+L)\rangle_{ab}(\gamma_3|c_2\rangle+\delta_3|c_1\rangle)]\\ &\otimes(\gamma_2|b_1\rangle+\delta_2|b_2\rangle)(|-1\rangle_{e_2}\gamma_1\beta_3|a_1L\rangle_{ac}\\ &+|+1\rangle_{e_2}\delta_1\beta_3|a_2L\rangle_{ac}-|-1\rangle_{e_2}\gamma_1\alpha_3|a_1L\rangle_{ac}\\ &+|+1\rangle_{e_2}\delta_1\alpha_3|a_2R\rangle_{ac}).\end{aligned} \tag{14}$$

After the Hadamard operations are performed on NV_1 and NV_2, we lead the wave packets of photon b from the two spatial modes $|b_1\rangle$ and $|b_2\rangle$ to H_P, CPBS, NV_1, CPBS, X, and U again (through the dotted line in Fig.5). And we lead those from the two spatial modes $|c_1\rangle$ and $|c_2\rangle$ to H_P, CPBS, NV_2, CPBS, X, and U (through the dotted line in Fig.5), and then the state of the quantum system becomes

$$\begin{aligned}|\Phi_{abce_1e_2}\rangle_7 = &[\alpha_1\beta_2|-1\rangle_{e_1}|RL\rangle_{ab}(\gamma_3|c_2\rangle+\delta_3|c_1\rangle)\\ &+\beta_1\beta_2|+1\rangle_{e_1}|LL\rangle_{ab}(\gamma_3|c_1\rangle+\delta_3|c_2\rangle)\\ &+\alpha_1\alpha_2|-1\rangle_{e_1}|RR\rangle_{ab}(\gamma_3|c_2\rangle+\delta_3|c_1\rangle)\\ &+\beta_1\alpha_2|+1\rangle_{e_1}|LR\rangle_{ab}(\gamma_3|c_2\rangle+\delta_3|c_1\rangle)]\\ &\otimes[\gamma_1\beta_3|+\rangle_{e_2}|a_1L\rangle_{ac}+\delta_1\beta_3|-\rangle_{e_2}|a_2L\rangle_{ac}\\ &-\frac{\gamma_1\alpha_3}{\sqrt{2}}|+\rangle_{e_2}|a_1(R-L)\rangle_{ac}\\ &-\frac{\delta_1\alpha_3}{\sqrt{2}}|+\rangle_{e_2}|a_2(R+L)\rangle_{ac}]\\ &\otimes(\gamma_2|b_1\rangle+\delta_2|b_2\rangle).\end{aligned} \tag{15}$$

After a Hadamard operation is performed on NV_2, we lead the wave packets of photon b from the two spatial modes $|b_1\rangle$ and $|b_2\rangle$ to CPBS, X, U, NV_2, U, X, and CPBS in sequence as shown in Fig.5. The state of the quantum system becomes

$$\begin{aligned}|\Phi_{abce_1e_2}\rangle_8 = &[\alpha_1\beta_2|-1\rangle_{e_1}|RL\rangle_{ab}(\gamma_3|c_2\rangle+\delta_3|c_1\rangle)\\ &+\beta_1\beta_2|+1\rangle_{e_1}|LL\rangle_{ab}(\gamma_3|c_1\rangle+\delta_3|c_2\rangle)\\ &+\alpha_1\alpha_2|-1\rangle_{e_1}|RR\rangle_{ab}(\gamma_3|c_2\rangle+\delta_3|c_1\rangle)\\ &+\beta_1\alpha_2|+1\rangle_{e_1}|LR\rangle_{ab}(\gamma_3|c_2\rangle+\delta_3|c_1\rangle)]\\ &\otimes[\gamma_1\beta_3|-1\rangle_{e_2}|a_1L\rangle_{ac}(\gamma_2|b_2\rangle+\delta_2|b_1\rangle)\\ &+\delta_1\beta_3|+1\rangle_{e_2}|a_2L\rangle_{ac}(\gamma_2|b_1\rangle+\delta_2|b_2\rangle)\\ &-\frac{\gamma_1\alpha_3}{\sqrt{2}}|-1\rangle_{e_2}|a_1(R-L)\rangle_{ac}(\gamma_2|b_2\rangle+\delta_2|b_1\rangle)\\ &-\frac{\delta_1\alpha_3}{\sqrt{2}}|-1\rangle_{e_2}|a_2(R+L)\rangle_{ac}(\gamma_2|b_2\rangle+\delta_2|b_1\rangle)].\end{aligned} \tag{16}$$

Next, after a Hadamard operation is performed on NV_2, we lead the wavep ackets from the two spatial modes $|c_1\rangle$ and $|c_2\rangle$ to CPBS, NV_2, CPBS, X, and U (through the dash-dot-dotted line in Fig.5). The state of the quantum system becomes

$$\begin{aligned}|\Phi_{abce_1e_2}\rangle_9 = &[|-1\rangle_{e_1}\alpha_1\beta_2|RL\rangle_{ab}(\gamma_3|c_2\rangle+\delta_3|c_1\rangle)\\ &+|+1\rangle_{e_1}\beta_1\beta_2|LL\rangle_{ab}(\gamma_3|c_1\rangle+\delta_3|c_2\rangle)\\ &+|-1\rangle_{e_1}\alpha_1\alpha_2|RR\rangle_{ab}(\gamma_3|c_2\rangle+\delta_3|c_1\rangle)\\ &+|+1\rangle_{e_1}\beta_1\alpha_2|LR\rangle_{ab}(\gamma_3|c_2\rangle+\delta_3|c_1\rangle)]\\ &\otimes[|+\rangle_{e_2}\gamma_1\beta_3|a_1L\rangle_{ac}(\gamma_2|b_2\rangle+\delta_2|b_1\rangle)\\ &+|-\rangle_{e_2}\delta_1\beta_3|a_2L\rangle_{ac}(\gamma_2|b_1\rangle+\delta_2|b_2\rangle)\\ &-\frac{\gamma_1\alpha_3}{\sqrt{2}}|+\rangle_{e_2}|a_1(R-L)\rangle_{ac}(\gamma_2|b_2\rangle+\delta_2|b_1\rangle)\\ &+\frac{\delta_1\alpha_3}{\sqrt{2}}|-\rangle_{e_2}|a_2(R+L)\rangle_{ac}(\gamma_2|b_2\rangle+\delta_2|b_1\rangle)].\end{aligned} \tag{17}$$

After another Hadamard operation is performed on NV_2 again, we put the wave packets of photon c from the two spatial modes $|c_1\rangle$ and $|c_2\rangle$ into H_P, CPBS, NV_2, CPBS, X, U, and CPBS (through the dotted line in Fig.5), and the state of the quantum system becomes

$$\begin{aligned}|\Phi_{abce_1e_2}\rangle_{10} = &[|-1\rangle_{e_1}\alpha_1\beta_2|RL\rangle_{ab}(\gamma_3|c_2\rangle+\delta_3|c_1\rangle)\\ &+|+1\rangle_{e_1}\beta_1\beta_2|LL\rangle_{ab}(\gamma_3|c_1\rangle+\delta_3|c_2\rangle)\\ &+|-1\rangle_{e_1}\alpha_1\alpha_2|RR\rangle_{ab}(\gamma_3|c_2\rangle+\delta_3|c_1\rangle)\\ &+|+1\rangle_{e_1}\beta_1\alpha_2|LR\rangle_{ab}(\gamma_3|c_2\rangle+\delta_3|c_1\rangle)]\\ &\otimes[|-1\rangle_{e_2}\gamma_1\beta_3|a_1L\rangle_{ac}(\gamma_2|b_2\rangle+\delta_2|b_1\rangle)\\ &+|+1\rangle_{e_2}\delta_1\beta_3|a_2L\rangle_{ac}(\gamma_2|b_1\rangle+\delta_2|b_2\rangle)\\ &+|-1\rangle_{e_2}\gamma_1\alpha_3|a_1R\rangle_{ac}(\gamma_2|b_2\rangle+\delta_2|b_1\rangle)\\ &+|+1\rangle_{e_2}\delta_1\alpha_3|a_2R\rangle_{ac}(\gamma_2|b_2\rangle+\delta_2|b_1\rangle)].\end{aligned} \tag{18}$$

At last, we perform a Hadamard operation on each of NV_1 and NV_2, and then the spatial-mode bit-flip operations are performed on photons b and c. By measuring the states of NV_1 and NV_2 with the orthogonal basis $\{|-1\rangle,|+1\rangle\}$, the outcome of the hybrid hyper-Toffoli gate on a three-photon system can be obtained by performing the conditional operations on photon a. If NV_1 is projected into the state $|+1\rangle_{e_1}$, a polarization operation $|L\rangle_a\rightarrow-|L\rangle_a$ is performed on photon a. If NV_2 is projected into the state $|+1\rangle_{e_2}$, a spatial-mode operation $|a_2\rangle\rightarrow-|a_2\rangle$ is performed on photon a. In this way, the state of the three-photon system abc becomes

$$\begin{aligned}|\Phi_{abc}\rangle = &[(\alpha_1\beta_2|RL\rangle_{ab}+\alpha_1\alpha_2|RR\rangle_{ab}+\beta_1\alpha_2|LR\rangle_{ab})\\ &(\gamma_3|c_1\rangle+\delta_3|c_2\rangle)+\beta_1\beta_2|LL\rangle_{ab}(\gamma_3|c_2\rangle+\delta_3|c_1\rangle)]\\ &[(\gamma_1\beta_3|a_1L\rangle_{ac}+\gamma_1\alpha_3|a_1R\rangle_{ac}+\delta_1\alpha_3|a_2R\rangle_{ac})\\ &(\gamma_2|b_1\rangle+\delta_2|b_2\rangle)+\delta_1\beta_3|a_2L\rangle_{ac}(\gamma_2|b_2\rangle+\delta_2|b_1\rangle)].\end{aligned} \tag{19}$$

This is the result of the hybrid hyper-Toffoli gate operating on the three-photon system abc.

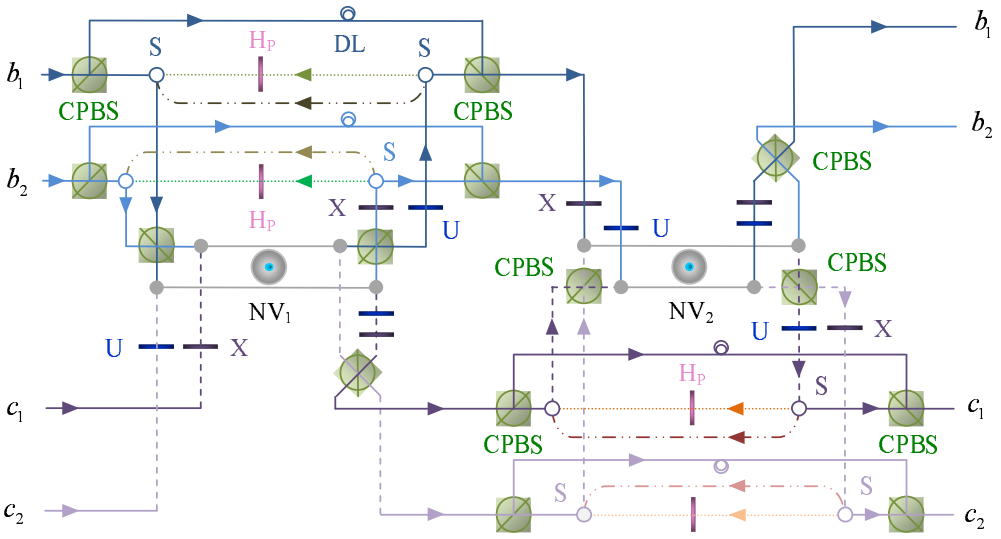

FIG. 5: (Color online) Schematic diagram for the second step of our hybrid photonic hyper-Toffoli gate operating on both the spatial-mode and polarization DOFs of a three-photon system. S represents an optical switch.

V. DISCUSSION AND SUMMARY

An NV center in diamond is an appropriate dipole emitter in cavity QED to obtain the high-fidelity reflection-transmission property in the Purcell regime, with its long spin coherence time (∼ms) [32, 36] and nanosecond manipulation time [37]. When a diamond NV center is coupled to a micro- or nano- cavity, the spontaneous emission of dipole emitter into the zero-phonon line can be greatly enhanced, and the interaction of the NV center and the photon is also enhanced [27, 28]. There are many experimental demonstrations of diamond NV centers coupled to micro- or nano- resonators with either a strong-coupling strength [25] or a weak-coupling one [26]. In 2012, Faraon *et al.* [28] demonstrated experimentally that the zero-phonon transition rate of an NV center is greatly enhanced (∼ 70) by coupling to a photonic crystal resonator ($Q \sim 3000$) fabricated in a monocrystalline diamond with the coupling strength as a few GHz, and they pointed out that the photonic crystal platform with a quality factor of $Q \sim 10^5$ can operate at the onset of strong-coupling regime.

In the double-sided cavity-NV-center system, the two waveguides are simultaneously coupled to the cavity resonator mode with the coupling constants η_1 and η_2, respectively. As the backscattering is low in the waveguide, the asymmetry of the two coupling constants is mainly caused by cavity intrinsic loss κ [20]. In experiment, the difference of the two coupling constants $\Delta\eta \sim 0.2\eta$ has been demonstrated, which yields approximately the same fidelity for both transmission and reflection directions [20]. The reflection and transmission coefficients of a double-sided cavity-NV-center system are dominated by the Purcell factor F_P and the cavity decay rate $\lambda = \kappa/\eta$. In the resonant condition ($\omega_c = \omega_k = \omega$), the transmission and reflection rule for a handedness circularly polarized light can be described as

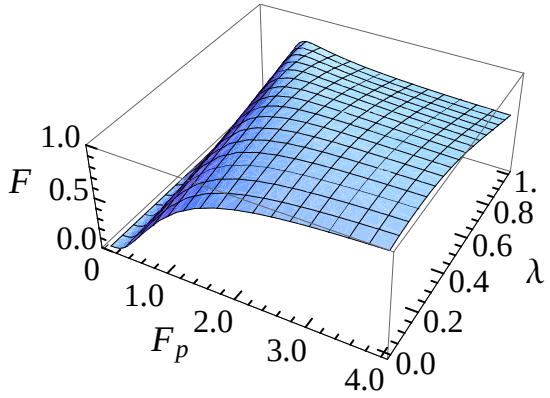

FIG. 6: (Color online) Fidelity (F) of a hybrid spatial-polarization hyper-CNOT gate vs the Purcell factor F_P and the cavity decay rate λ.

$$
\begin{aligned}
|R^{\uparrow},-1\rangle &\rightarrow |rL^{\downarrow}+tR^{\uparrow},-1\rangle,\\
|L^{\downarrow},-1\rangle &\rightarrow |rR^{\uparrow}+tL^{\downarrow},-1\rangle,\\
|R^{\downarrow},+1\rangle &\rightarrow |rL^{\uparrow}+tR^{\downarrow},+1\rangle,\\
|L^{\uparrow},+1\rangle &\rightarrow |rR^{\downarrow}+tL^{\uparrow},+1\rangle,\\
|R^{\downarrow},-1\rangle &\rightarrow |t_0R^{\downarrow}+r_0L^{\uparrow},-1\rangle,\\
|L^{\uparrow},-1\rangle &\rightarrow |t_0L^{\uparrow}+r_0R^{\downarrow},-1\rangle,\\
|R^{\uparrow},+1\rangle &\rightarrow |t_0R^{\uparrow}+r_0L^{\downarrow},+1\rangle,\\
|L^{\downarrow},+1\rangle &\rightarrow |t_0L^{\downarrow}+r_0R^{\uparrow},+1\rangle.
\end{aligned}
\tag{20}
$$

The fidelity of the photonic quantum logic gate can be calculated by $F = \overline{|\langle\psi_f|\psi\rangle|^2}$, where $|\psi\rangle$ is the ideal finial state of a quantum logical gate, and $|\psi_f\rangle$ is the finial

state of a quantum system by considering experimental factors ($\alpha_i, \beta_i, \gamma_i, \delta_i \in [0,1]$). The fidelity of our hybrid photonic hyper-CNOT gate is shown in Fig.6, which is decreased with a small Purcell factor or a large cavity intrinsic loss. In Fig.6, the fidelity of the hybrid photonic hyper-CNOT gate is higher with a small Purcell factor when the cavity intrinsic loss becomes larger, which corresponds to the regime $|r| \simeq |t_0|$. That is, the fidelity of the hybrid photonic hyper-CNOT gate is higher when the reflection-transmission properties of the uncoupled cavity and the coupled cavity are symmetrical. In the case $|r| = |t_0|$, the relation of the Purcell factor and the cavity decay rate is $F_P = (1 - \frac{\lambda^2}{4})/\lambda$.

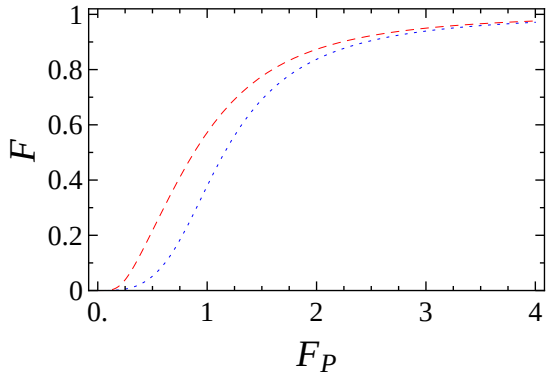

FIG. 7: (Color online) Fidelity (F) of a hybrid spatial-polarization hyper-CNOT gate on a two-photon system (red dashed line) and that of two identical polarization CNOT gates on a four-photon system (blue dotted line) vs the Purcell factor F_P. Here the cavity decay rate is chosen as $\lambda = 0.1$, and the construction of the polarization CNOT gate is the same as that of the polarization part of the hyper-CNOT gate in Ref. [13].

The probability of recovering an incident photon after operation is increased with a large cavity decay rate η [20]. O'Shea *et al.* [20] noted that the maximal fidelity of the operation with cavity QED is achieved at the regime where the coupling strength g is smaller than the cavity decay rate η ($F_P > 1$) rather than the strong-coupling regime, and the maximal fidelity is obtained at the point $\lambda \simeq 0.1$ in their experiment. In the case $\lambda = 0.1$, the fidelity of our hybrid photonic hyper-CNOT gate on a two-photon system and that of the two identical CNOT gates on a four-photon system in one DOF are shown in Fig.7. It shows that the fidelity of our hybrid photonic hyper-CNOT gate is higher than the one for the two CNOT gates in one DOF in the weak-coupling regime with a small Purcell factor. In the case $|r| = |t_0|$, the fidelity of the hybrid hyperparallel photonic logic gate is equal to the one for the two identical photonic logic gates in one DOF (e.g., the fidelity of the hybrid hyper-Toffoli gate shown in Fig.8). In the case $\lambda = 0.1$ and $F_P = 9.875$, both the fidelity of the hybrid photonic hyper-CNOT gate and that of the two identical CNOT gates in one DOF are $F = 99.7\%$. That is, the hybrid hyperparallel photonic logic gate can decrease the effect of environment noise in the asymmetric condition of the double-sided cavity-NV-center system in the weak-coupling regime with a small Purcell factor.

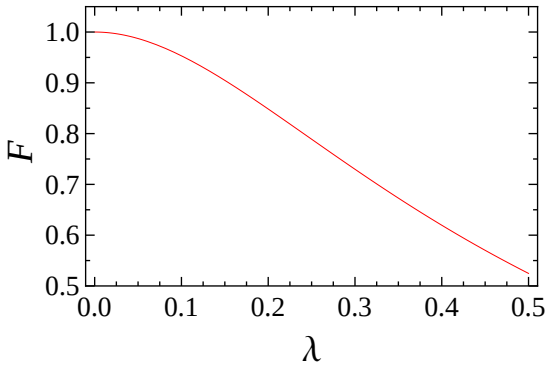

FIG. 8: (Color online) Fidelity (F) of a hybrid spatial-polarization hyper-Toffoli gate vs the cavity decay rate λ in the case $|r| = |t_0|$ [$F_P = (1 - \frac{\lambda^2}{4})/\lambda$], which is equal to the one for two polarization Toffoli gates on a six-photon system.

The reflection property of one-sided dipole-cavity protocols is fragile because the reflectance for the uncoupled cavity and the coupled cavity should be balanced to get a high fidelity, while the reflection-transmission property of double-sided dipole-cavity systems is robust and flexible with the large reflectance and transmittance difference between the uncoupled cavity and the coupled cavity [12, 13]. Moreover, a double-sided dipole-cavity system has two spatial modes, so it is very convenient to use this DIT to investigate the robust and flexible quantum information processing based on the polarization and spatial-mode DOFs of photon systems.

Both CONT and Toffoli gates are parts of the set of universal quantum logic gates, and they can form universal quantum computing with the assistance of single-qubit rotation gates [1]. Both our hybrid polarization-spatial hyper-CNOT gate and hyper-Toffoli gate can form universal hyperparallel photonic quantum computing assisted by the rotations on a single photon in two DOFs, which is useful in the quantum information protocols with multi-qubit systems in several DOFs. For example, hyperentanglement is useful in quantum communication protocols for increasing the channel capacity [38], resorting to the entanglement in several DOFs of photon systems [39]. With hyperparallel quantum gates, the generation and complete analysis of hyperentangled states can be achieved in a relatively simpler way, compared with the protocols with several cascaded quantum entangling gates [40–42]. Besides, some quantum information processes can be implemented with less resources based on several DOFs of photon systems, resorting to the hyperparallel quantum gates. For example, in the preparation of four-qubit cluster states, only a hyper-CNOT gate operation (photons interact with electron spins four times) and a wave plate are required in the protocol with two photons in two DOFs [43], while three

CNOT gate operations (photons interact with electron spins six times) are required in the protocol with four photons in one DOF.

In summary, we have presented the DIT of a double-sided cavity-NV-center system, which is still obvious in the weak-coupling regime. The reflection-transmission property of circularly polarized light interacting with a double-sided cavity-NV-center system can be used for photon-photon interaction in quantum information processing based on both the polarization and spatial-mode DOFs. With the DIT of double-sided cavity-NV-center systems, we have proposed a hybrid photonic hyper-CNOT gate and a hybrid photonic hyper-Toffoli gate for hyperparallel photonic quantum computation. A hyperparallel hybrid quantum logic gate on a quantum system in both the polarization and spatial-mode DOFs is equal to the two identical quantum gates operating on that in one DOF simultaneously, and it can depress the resource consumption, photonic dissipation, and asymmetric environment noise of the double-sided cavity-NV-center system in the weak-coupling regime with a small Purcell factor. Besides, these hyperparallel quantum logic gates are useful for the quantum information protocols with multi-qubit systems in several DOFs, especially the generation and analysis of hyperentangled states [40–42].

The double-sided cavity QED can be used for quantum information processing even in a bad cavity regime (the Purcell regime) [12, 13, 19], and it is suitable to investigate the robust and flexible quantum information processing based on both the polarization and spatial-mode DOFs [40–42], according to its reflection-transmission optical property. Besides the quantum computation with two DOFs of a photon as two qubits [44, 45], double-sided cavity QED can also be used for quantum information processing with two DOFs by using a photon as a qudit. Moreover, the multiqubit logic gate based on one DOF can be simplified with less photon resources by resorting to two DOFs of photon systems [46].

ACKNOWLEDGMENTS

This work is supported by the National Natural Science Foundation of China under Grants Nos. 11174039 and 11474026, and NECT-11-0031.

[1] M. A. Nielsen and I. L. Chuang, *Quantum Computation and Quantum Information* , Cambridge University Press, Cambridge, (2000).

[2] Y. Makhlin, G. Schön, and A. Shnirman, Rev. Mod. Phys. **73**, 357 (2001); L. M. K. Vandersypen and I. L. Chuang, Rev. Mod. Phys. **76**, 1037 (2005); P. Kok, W. J. Munro, K. Nemoto, T. C. Ralph, J. P. Dowling, and G. J. Milburn, Rev. Mod. Phys. **79**, 135 (2007); L. M. Duan and C. Monroe, Rev. Mod. Phys. **82**, 1209 (2010).

[3] F. Schmidt-Kaler, H. Häffner, M. Riebe, S. Gulde, G. P. T. Lancaster, T. Deuschle, C. Becher, C. F. Roos, J. Eschner, and R. Blatt, Nature (London) **422**, 408 (2003).

[4] N. A. Gershenfeld and I. L. Chuang, Science **275**, 350 (1997); G. Feng, G. Xu, and G. Long, Phys. Rev. Lett. **110**, 190501 (2013).

[5] X. Li, Y. Wu, D. Steel, D. Gammon, T. H. Stievater, and D. S. Katzer, Science **301**, 809 (2003); H. R. Wei and F. G. Deng, Sci. Rep. **4**, 7551 (2014).

[6] T. Yamamoto, Y. A. Pashkin, O. Astafiev, Y. Nakamura and J. S. Tsai, Nature (London) **425**, 941 (2003); A. Blais, R. S. Huang, A. Wallraff, S. M. Girvin, R. J. Schoelkopf, Phys. Rev. A **69**, 062320 (2004); M. Hua, M. J. Tao, and F. G. Deng, Phys. Rev. A **90**, 012328 (2014); M. Hua, M. J. Tao, and F. G. Deng, Sci. Rep. **5**, 9274 (2015).

[7] E. Knill, R. Laflamme, and G. J. Milburn, Nature (London), **409**, 46 (2001); J. L. O'Brien, G. J. Pryde, A. G. White, T. C. Ralph, and D. Branning, Nature (London) **426**, 264 (2003).

[8] K. Nemoto and W. J. Munro, Phys. Rev. Lett. **93**, 250502 (2004).

[9] L. M. Duan and H. J. Kimble, Phys. Rev. Lett. **92**, 127902 (2004); H. R. Wei and F. G. Deng, Opt. Express **21**, 17671 (2013).

[10] A. Rauschenbeutel, G. Nogues, S. Osnaghi, P. Bertet, M. Brune, J. Raimond, and S. Haroche, Science **288**, 2024 (2000).

[11] C. Y. Hu, A. Young, J. L. O'Brien, W. J. Munro, and J. G. Rarity, Phys. Rev. B **78**, 085307 (2008).

[12] E. Waks and J. Vuckovic, Phys. Rev. Lett. **96**, 153601 (2006); C. Y. Hu, W. J. Munro, J. L. O'Brien, and J. G. Rarity, Phys. Rev. B **80**, 205326 (2009).

[13] C. Bonato, F. Haupt, S. S. R. Oemrawsingh, J. Gudat, D. Ding, M. P. van Exter, and D. Bouwmeester, Phys. Rev. Lett. **104**, 160503 (2010); B. C. Ren and F. G. Deng, Sci. Rep. **4**, 4623 (2014).

[14] B. C. Ren, H. R. Wei, and F. G. Deng, Laser Phys. Lett. **10**, 095202 (2013).

[15] T. Wilk, S. C. Webster, A. Kuhn, and G. Rempe, Science **317**, 488 (2007); B. Weber, H. P. Specht, T. Müller, J. Bochmann, M. Mücke, D. L. Moehring, and G. Rempe, Phys. Rev. Lett. **102**, 030501 (2009); K. Hammerer, A. S. Sørensen, and E. S. Polzik, Rev. Mod. Phys. **82**, 1041 (2010).

[16] C. Junge, D. O'Shea, J. Volz, and A. Rauschenbeutel, Phys. Rev. Lett. **110**, 213604 (2013).

[17] A. Reiserer, N. Kalb, G. Rempe, and S. Ritter, Nature (London) **508**, 237 (2014); I. Shomroni, S. Rosenblum, Y. Lovsky, O. Bechler, G. Guendelman, B. Dayan, Science **345**, 903 (2014).

[18] E. M. Purcell, H. C. Torrey, and R. V. Pound, Phys. Rev. **69**, 37 (1946); J. M. Gérard, B. Sermage, B. Gayral, B. Legrand, E. Costard, and V. Thierry-Mieg, Phys. Rev. Lett. **81**, 1110 (1998); A. Auffèves-Garnier, C. Simon, J. M. Gérard, and J. P. Poizat, Phys. Rev. A **75**, 053823 (2007).

[19] J. T. Shen and S. Fan, Opt. Lett. **30**, 2001 (2005); Y. Li, L. Aolita, D. E. Chang, and L. C. Kwek, Phys. Rev.

Lett. **109**, 160504 (2012).
[20] D. O'Shea, C. Junge, J. Volz, and A. Rauschenbeutel, Phys. Rev. Lett. **111**, 193601 (2013).
[21] E. Waks and J. Vuckovic, Phys. Rev. A **73**, 041803(R) (2006); I. Fushman, D. Englund, A. Faraon, N. Stoltz, P. Petroff, and J. Vučković, Science **320**, 769 (2008); T. G. Tiecke, J. D. Thompson, N. P. de Leon, L. R. Liu, V. Vuletić, and M. D. Lukin, Nature (London) **508**, 241 (2014).
[22] P. Neumann, N. Mizuochi, F. Rempp, P. Hemmer, H. Watanabe, S. Yamasaki, V. Jacques, T. Gaebel, F. Jelezko, and J. Wrachtrup, Science **320**, 1326 (2008); G. D. Fuchs, G. Burkard, P. V. Klimov, and D. D. Awschalom, Nat. Phys. **7**, 789 (2011).
[23] A. Young, C. Y. Hu, L. Marseglia, J. P. Harrison, J. L. O'Brien, and J. G. Rarity, New J. Phys. **11**, 013007 (2009); Q. Chen, W. Yang, M. Feng, and J. Du, Phys. Rev. A **83**, 054305 (2011); A. Zheng, J. Li, R. Yu, X. Y. Lü, and Y. Wu, Opt. Express **20**, 16902 (2012); H. R. Wei and F. G. Deng, Phys. Rev. A **88**, 042323 (2013).
[24] Y. S. Park, A. K. Cook, and H. Wang, Nano Lett. **6**, 2075 (2006); D. Englund, B. Shields, K. Rivoire, F. Hatami, J. Vučković, H. Park, and M. D. Lukin, Nano Lett. **10**, 3922 (2010); J. Wolters, A. W. Schell, G. Kewes, N. Nüsse, M. Schoengen, H. Döscher, T. Hannappel, B. Löchel, M. Barth, and O. Benson, Appl. Phys. Lett. **97**, 141108 (2010); O. Arcizet, V. Jacques, A. Siria, P. Poncharal, P. Vincent, and S. Seidelin, Nat. Phys. **7**, 879 (2011).
[25] P. E. Barclay, K. M. Fu, C. Santori, and R. G. Beausoleil, Opt. Express **17**, 9588 (2009).
[26] P. E. Barclay, K. M. C. Fu, C. Santori, and R. G. Beausoleil, Appl. Phys. Lett. **95**, 191115 (2009).
[27] A. Faraon, C. Santori, Z. Huang, V. M. Acosta, and R. G. Beausoleil, Phys. Rev. Lett. **109**, 033604 (2012).
[28] A. Faraon, P. E. Barclay, C. Santori, K. M. C. Fu, and R. G. Beausoleil, Nat. Photonics **5**, 301 (2011); P. E. Barclay, K. M. C. Fu, C. Santori, A. Faraon, and R. G. Beausoleil, Phys. Rev. X. **1**, 011007 (2011).
[29] R. Hanson, V. V. Dobrovitski, A. E. Feiguin, O. Gywat, and D. D. Awschalom, Science **320**, 352 (2008); P. Neumann, R. Kolesov, B. Naydenov, J. Beck, F. Rempp, M. Steiner, V. Jacques, G. Balasubramanian, M. L. Markham, D. J. Twitchen, S. Pezzagna, J. Meijer, J. Twamley, F. Jelezko, and J. Wrachtrup, Nat. Phys. **6**, 249 (2010).
[30] L. Childress, M. V. G. Dutt, J. M. Taylor, A. S. Zibrov, F. Jelezko, J. Wrachtrup, P. R. Hemmer, and M. D. Lukin, Science **314**, 281 (2006); P. Neumann, J. Beck, M. Steiner, F. Rempp, H. Fedder, P. R. Hemmer, J. Wrachtrup, and F. Jelezko, Science **329**, 542 (2010).
[31] E. Togan, Y. Chu, A. S. Trifonov, L. Jiang, J. Maze, L. Childress, M. V. G. Dutt, A. S. Sørensen, P. R. Hemmer, A. S. Zibrov, and M. D. Lukin, Nature (London) **466**, 730 (2010).
[32] B. B. Buckley, G. D. Fuchs, L. C. Bassett, and D. D. Awschalom, Science **330**, 1212 (2010).
[33] A. Lenef and S. C. Rand, Phys. Rev. B **53**, 13441 (1996).
[34] D. F. Walls and G. J. Milburn, *Quantum Optics*, Springer-Verlag, Berlin, (1994).
[35] H. R. Wei and F. G. Deng, Phys. Rev. A **87**, 022305 (2013).
[36] G. Balasubramanian, P. Neumann, D. Twitchen, M. Markham, R. Kolesov, N. Mizuochi, J. Isoya, J. Achard, J. Beck, J. Tissler, V. Jacques, P. R. Hemmer, F. Jelezko, and J. Wrachtrup, Nat. Mater. **8**, 383 (2009).
[37] G. D. Fuchs, V. V. Dobrovitski, D. M. Toyli, F. J. Heremans, and D. D. Awschalom, Science **326**, 1520 (2009).
[38] J. T. Barreiro, T. C. Wei, and P. G. Kwiat, Nature Phys. **4**, 282 (2008).
[39] J. T. Barreiro, N. K. Langford, N. A. Peters, and P. G. Kwiat, Phys. Rev. Lett. **95**, 260501 (2005); G. Vallone, R. Ceccarelli, F. De Martini, and P. Mataloni, Phys. Rev. A **79**, 030301(R) (2009).
[40] Y. B. Sheng, F. G. Deng, and G. L. Long, Phys. Rev. A **82**, 032318 (2010).
[41] B. C. Ren, H. R. Wei, M. Hua, T. Li, and F. G. Deng, Opt. Express **20**, 24664 (2012).
[42] T. J. Wang, Y. Lu, and G. L. Long, Phys. Rev. A **86**, 042337 (2012).
[43] B. C. Ren, F. F. Du, and F. G. Deng, Phys. Rev. A **88**, 012302 (2013).
[44] M. Scholz, T. Aichele, S. Ramelow, and O. Benson, Phys. Rev. Lett. **96**, 180501 (2006); P. Zhang, R. F. Liu, Y. F. Huang, H. Gao, and F. L. Li, Phys. Rev. A **82**, 064302 (2010); C. Vitelli, N. Spagnolo, L. Aparo, F. Sciarrino, E. Santamato, and L. Marrucci, Nat. Photonics **7**, 521 (2013).
[45] N. Yoran and B. Reznik, Phys. Rev. Lett. **91**, 037903 (2003); A. F. Abouraddy, G. Di Giuseppe, T. M. Yarnall, M. C. Teich, and B. E. A. Saleh, Phys. Rev. A **86**, 050303(R) (2012).
[46] T. J. Wang, Y. Zhang, and C. Wang, Laser Phys. Lett. **11**, 025203 (2014).